Journal of Structural Geology 31 (2009) 92–103

Contents lists available at ScienceDirect

Journal of Structural Geology

journal homepage: www.elsevier.com/locate/jsg

Microstructural analysis of anhydrite rocks from the Triassic Evaporites, Umbria-Marche Apennines, Central Italy: An insight into deformation mechanisms and possible slip systems

Rebecca C. Hildyard*, David J. Prior, Daniel R. Faulkner, Elisabetta Mariani

Department of Earth and Ocean Sciences, University of Liverpool, 4 Brownlow Street, Liverpool, L69 3GP, UK

ARTICLE INFO

Article history:
Received 24 June 2008
Received in revised form
20 October 2008
Accepted 23 October 2008
Available online 31 October 2008

Keywords:
Anhydrite
Misorientation analysis
Slip systems
Microstructure

ABSTRACT

Anhydrite-rich layers within foreland fold and thrust belts are frequently the weakest horizon of the sequence. Characterizing the microstructural textures of anhydrite is therefore important for interpreting the larger scale deformation history of these rocks. The microstructure of naturally deformed anhydrite from the Triassic Evaporites of the Umbria-Marche Apennines, Italy has been analyzed using electron backscatter diffraction (EBSD). This technique has been used to measure the misorientation across distorted grains and the crystallographic preferred orientation (CPO) of the samples. The reference frame of the standard space group Cmcm was used to represent the structure of anhydrite during this analysis which is different to that used in previous studies. Some grains show significant intracrystalline distortions (4 –18° misorientation). Lines of measurements across distortions showed a dispersion of crystallographic data around a clear misorientation axis [010]. These data are combined with the trace orientations of distortions to confirm that the (100)[001] slip systems previously recognized also best explains grain distortions. These interpretations are based on, and consistent with, a tilt boundary model containing edge dislocations. CPO data are also interpreted as a likely (100)[001] slip system, as has previously been recognized. A high degree of twinning within many of the anhydrite grains apparently has little effect on the crystallographic textures observed.

1. Introduction

Evaporitic rocks have been recognized to act as detachment horizons in many fold and thrust belts globally, including the Northern Apennines in Italy (Bally et al., 1986; Barchi et al., 1998a), the Jura Mountains of Switzerland (Laubscher, 1975; Jordan and Nuesch, 1989) and the Antalya Thrust system in southern Turkey (Marcoux et al., 1987). The deformation in these zones is largely thought to be plastic (i.e. accommodated by viscous processes such as dislocation and diffusion creep) but brittle deformation also occurs. For example, it has recently been observed that the main shocks of the 1997 Colfiorito earthquake sequence in the Umbria-Marche Apennines were nucleated on normal faults within the Triassic Evaporites (Barchi et al., 1998a; Miller et al., 2004) (see Fig. 1). Detailed meso and large scale studies on the brittle fault zone architecture within the Triassic Evaporites have found that pre-existing syn-orogenic plastic deformation fabrics have strongly controlled the brittle fault zone geometry (De Paola et al., 2008).

The impetus and basis for this work is to provide a detailed microstructural study of anhydrites found in the Triassic Evaporite sequence recovered from boreholes at depth. This will provide constraints on the plastic deformation mechanisms and operative slip systems, before further work on the general and regional geological implications can be carried out.

Relatively few microstructural studies have been made of naturally deformed anhydrite. Anhydrite has orthorhombic crystal symmetry. Early authors (Mugge, 1883; Ramez, 1976b) used a crystal setting of space group Bbmm as a reference frame for their crystallographic data, therefore subsequent authors (i.e. Mainprice et al., 1993; Dell'Angelo and Olgaard, 1995; Heidelbach et al., 2001) have adhered to this convention for comparison purposes. Due in part to software constraints, this work uses the standard setting for anhydrite which is the space group Cmcm, transformed from the space group Amma, which is considered to be the most accurate setting for anhydrite (Cheng and Zussman, 1963; Hawthorne and Ferguson, 1975) and therefore, from this point, all previously published crystallographic planes, directions and slip systems have been rotated into this reference frame for continuity and comparison purposes (for further details see Section 3.3 and Appendix A). For data presented in its original reference frame see Table 2. Early

* Corresponding author. Fax: +44 151 794 5169.
E-mail address: rebecca.hildyard@liverpool.ac.uk (R.C. Hildyard).

0191-8141/$ – see front matter © 2008 Elsevier Ltd. All rights reserved.
doi:10.1016/j.jsg.2008.10.009

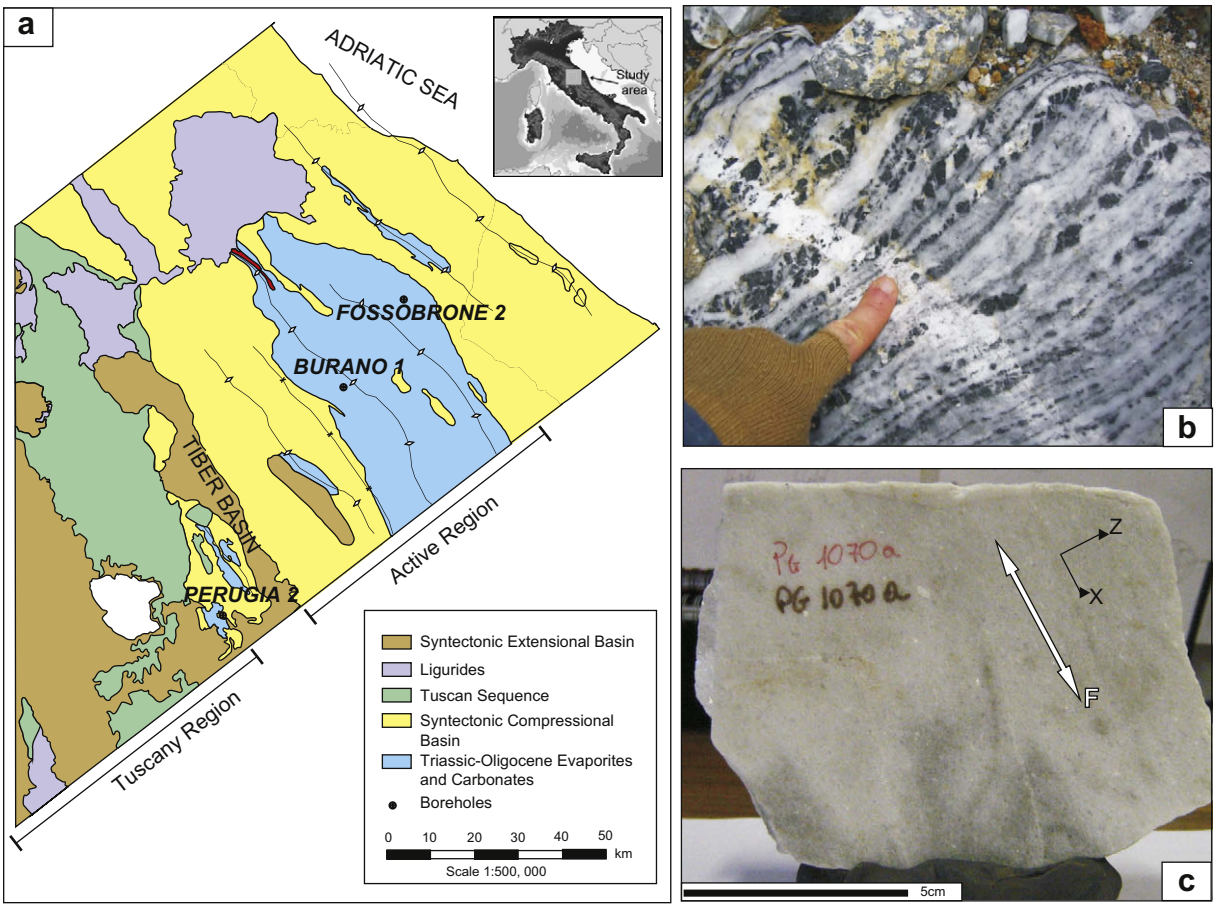

Fig. 1. (a) Summary map of the main geological units, and borehole locations from which the samples analyzed in this study were cored; (b) surface exposure of the Triassic Evaporites showing the light coloured, foliated Ca-sulphate (gypsum) and dark, fractured dolomite layers (taken from De Paola et al., 2008); (c) core sample prior to cutting, arrow indicated to the foliation outline by a shape preferred orientation of anhydrite, the slightly darker bands seen are horizons with higher dolomite concentrations than other areas. *Z*–*X* indicate the reference frame for each sample with *X* parallel to foliation.

authors (Mugge, 1883; Ramez, 1976b) recognized from bulk crystallographic preferred orientation (CPO) analyses that three general intracrystalline deformation mechanisms and slip systems were active for anhydrite: (1) translation glide on (100)[001]; (2) translation glide on (201)[1-1-2] and [11-2]; (3) twinning on {110} (a rotation of the [100] axis by 83.5° around [001]; (Klassen-Neklyudova, 1964)). These are represented in Fig. 2. More recently Mainprice et al. (1993) used neutron diffraction texture goniometry to determine the dominant deformation mechanism of (100)[001] glide within naturally deformed anhydrite. The texture analysis found that the CPO observed was also consistent with slip on {201}⟨112⟩. Mainprice et al. (1993) showed that in the samples they analyzed deformation twinning contributed to the development of a strong CPO.

In triaxial deformation experiments ($\sigma_1 > \sigma_2 = \sigma_3$) on fine grained anhydrite aggregates between 400 °C and 800 °C and confining pressures of 150–300 MPa, two high temperature flow regimes were recognized (Dell'Angelo and Olgaard, 1995). Within regime (1) deformation microstructures (i.e. twins, undulose extinction, grain flattening, serrate grain and twin boundaries, high dislocation densities identified by TEM analysis and newly recrystallized strain free grains) were explained by twinning and dislocation creep mechanisms at high stresses, while in regime (2) very little microstructural evidence of bulk deformation (i.e. a random CPO and significant grain boundary relief) was attributed to diffusion creep with grain boundary sliding at low stresses. It was also suggested that a CPO reflected twinning at low strains and a combination of slip systems at high strains. Further experimental results conducted on polycrystalline anhydrite deformed in torsion (Heidelbach et al., 2001) investigated the development of CPO as a function of shear strain/shear strain rate using a small synchrotron X-ray beam to perform diffraction experiments in transmission geometry. It was found that the formation of a deformation CPO starts at shear strains of 1.5–2.6 and that as the strain was increased, and a change from dislocation to diffusion controlled creep occurs, the CPO is actually strengthened rather than weakened. The CPO found in this study was very similar to those observed in naturally deformed samples and it was suggested that these could be explained by activity on the (100)⟨001⟩ and (201)⟨112⟩ slip systems.

As a CPO of a material directly records the result of a reorientation of crystal lattices by dislocation motion in specific crystallographic planes and directions (Wenk and Bulakh, 2004), slip systems inferred from CPOs will reflect the systems that have been most active during deformation: the easiest slip system. Misorientation analysis is another method that can be used to determine crystallographic slip systems (Lloyd and Freeman, 1991; Lloyd et al., 1997; Leiss and Barber, 1999; Prior, 1999; Prior et al., 2002). This technique considers the relationships between the crystal slip system responsible for a given rotation and misorientation between adjacent regions and the orientation of the boundary separating them (Lloyd et al., 1997). By using small circle dispersions of crystallographic planes/directions within deformed crystals and applying certain geometrical assumptions as to the nature

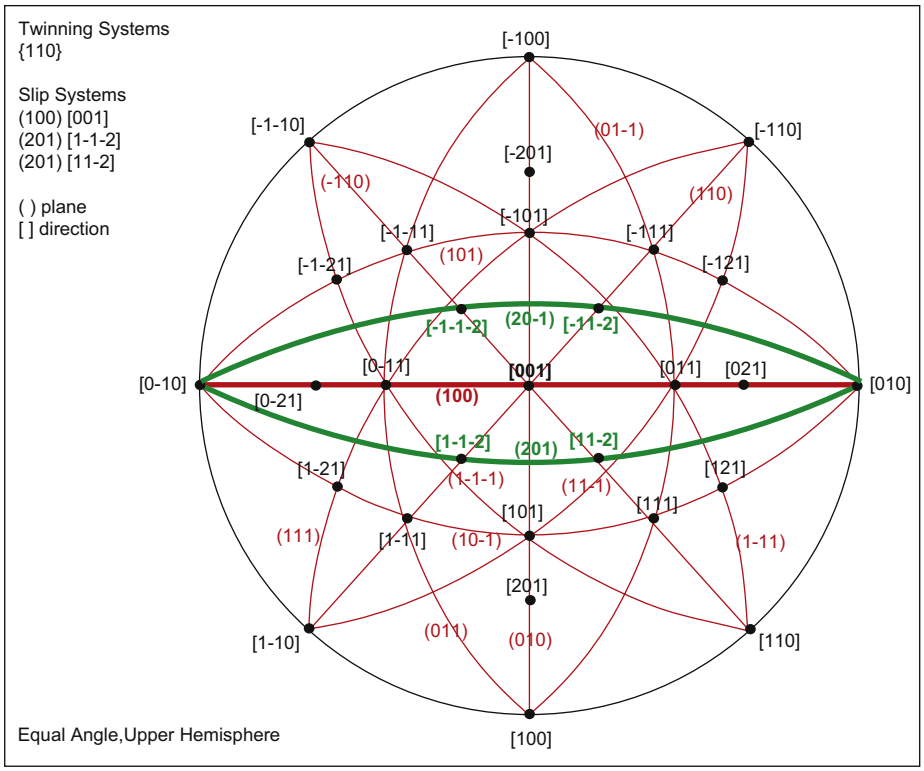

Fig. 2. Stereographic projection (equal angle, upper hemisphere) of orthorhombic anhydrite, showing important planes and directions and known slip systems and twin planes. Bold lines and text indicate the listed slip systems. The {201}⟨112⟩ slip systems (green slip plane and directions) actually plot on the lower hemisphere therefore these planes and directions are displayed in a lower hemisphere orientation.

of the boundaries and the types of dislocations present, it is possible to constrain the slip systems that are likely to have been active. When this method is applied to lattice distortions within individual grains an inference about all slip systems, including those which were less dominant, can be made.

The work presented here shows that by using EBSD as a novel approach to measure the full crystallographic orientation of anhydrite samples and analyzing the data for grain distortions, CPO and twinning, we can confirm previously recognized slip systems active within anhydrite and show that misorientation analysis is a powerful tool for identifying slip systems within anhydrite.

2. Samples

The samples used in this study are foliated anhydrite-rich (~95%) rocks from the Perugia 2 borehole located within the Triassic –Oligocene evaporites and carbonates of the Umbria-Marche region of the Apennines in central Italy (Fig. 1). The region has experienced two phases of deformation (Elter et al., 1975; Jolivet et al., 1998; Pauselli et al., 2006) an early Cretaceous to Quaternary shortening and thrusting and a later Miocene to recent post-collisional extensional phase. The extensional tectonics of the area have migrated with time from west to east. The extension has allowed the study of exhumed compressional deformation in addition to evaporite bearing normal faults exposed at the surface (e.g. De Paola et al., 2008). However, surface exposures have little anhydrite left as hydration reactions have replaced it with gypsum. Hence, in order to study primary anhydrite deformation, subsurface samples must be used. The core samples used here are from the actively extending region (Fig. 1a) and are taken from a depth of 1070 m in the Triassic Evaporite sequence. Due to the nature of core samples these specimens are unorientated and way up is not known, however the cores were drilled vertically and therefore it can be noted that the foliation dips between 40 and 60° from horizontal. Fig. 1c shows the core sample prior to cutting. In hand specimens, a clear shape preferred orientation of the anhydrite

Table 1
Summary table of the samples used in this study: (a) optical properties; (b) EBSD information.

(a)	Sample no.	Mineral phases present		XRD analysis of anhydrite content (%)	Grain size	Grain size range (μm)	Foliation
	PG1070a.1	Anhydrite; dolomite		>95	Coarse	10–460	Yes
	PG1070a.2	Anhydrite; dolomite		>95	Coarse	10–474	Yes
	PG1070b.1	Anhydrite; dolomite		>95	Coarse	10–1070	Yes
	PG1070b.2	Anhydrite; dolomite		>95	Coarse	10–720	Yes
(b)	EBSD map no.	Grain distortion magnification	Grain distortion step size (μm)	CPO magnification	CPO step size (μm)	CPO sample size (based on 1 point per grain	M-index for strength of texture
	PG1070a.1	×150	4	×50	25	258	0.1438
	PG1070a.2	×150	3	×50	25	1190	0.1293
	PG1070b.1	×200	2	×50	25	613	0.0968
	PG1070b.2	×200	2	×50	25	1087	0.0885

Table 2
Summary of slip systems from previous work, the rotated equivalents of previous work and the slip system from this work.

Slip systems from previous work (e.g. Muller et al., 1981)	Previous slip systems converted in to current ref. frame	Slips systems from this work
(001)[010]	(100)[001]	(100)[001]
(012)[-1-21]	(201)[1-1-2]	
(012)[1-21]	(201)[11-2]	

crystals defines the foliation, however there is no lineation, therefore these samples can be referred to as S-tectonites. Grain shape is defined as being essentially pancake (oblate) shaped, suggesting that a flattening strain has been involved in the deformation of these rocks. The samples are coarse grained and appears to be pure anhydrite.

3. Methods

3.1. Sample preparation

Two mutually perpendicular sections (perpendicular to foliation) were cut from two parts of a core. The rock chips were then made into to 30 μm thick polished thin sections. The use of water was excluded during the preparation of the thin sections to avoid any hydration of the anhydrite. Only in the final stages of chemo-mechanical polishing was water based SYTON used for very short time intervals (15 min for each sample). BSE imaging of the samples was used to confirm that no hydration of the anhydrite had occurred during preparation. Finally the samples were coated in a thin film of carbon to prevent charging.

3.2. Data acquisition

All anhydrite crystallographic orientation data were collected using a Philips XL30 SEM with a tungsten filament. In order to perform EBSD, samples are rotated to 70° from horizontal whilst the electron beam is vertical. The EBSD patterns were collected using an accelerating voltage of 20 kV and beam current of 3 nA. The working distance between sample and pole piece was 24 mm. Samples were 'mapped' using automated beam scanning, where the specimen is stationary and the beam scans a user defined area. The stage then drives to a new area and the beam scanning is resumed. For bulk CPO analysis low magnification (×50) large step size (25 μm) maps were made whereas for more detailed textural analysis (such as for grain distortions) high magnification (between ×150 and ×200) small step size (2–4 μm) maps were collected (see Table 1b for summary). All EBSD raw data are post processed using the HKL Technology manufacturer's software package Channel5 (Schmidt and Olesen, 1989). Non-indexed and mis-indexed points (such as one point indexed as dolomite in a large grain dominated by anhydrite) were carefully removed in a systematic way such that the overall data set remained accurate. Samples yielded 75 –80% correct indexing prior to processing and >90% after processing.

3.3. Unit cell setting

Anhydrite has orthorhombic crystal symmetry belonging to point group 2/m 2/m 2/m. The standard space group used to describe the structure of the crystal is Cmcm with basis vectors *a b c*. Due to the similarity in length of crystal axis authors have used three different space groups to best describe the structure; Bbmm (basis vectors *b c a*) (e.g. Hohne, 1963); Amma (basis vectors *c a b*) (e.g. Hawthorne and Ferguson, 1975); and Bmmb (basis vectors *a −c b*) (e.g. Hartman, 1989). Previous textural studies on anhydrite rocks have used the space group Bbmm (i.e. Mainprice et al., 1993; Dell'Angelo and Olgaard, 1995; Heidelbach et al., 2001) with a unit cell of $a = 6.238$ Å $b = 6.992$ Å $c = 6.998$ Å. The work presented here uses the standard space group Cmcm with crystal axis $a = 6.995$ Å $b = 6.245$ Å $c = 6.993$ Å. This is due to constraints within the Channel5 software (see Appendix A for further details) the result of which is that the data presented here is not directly comparable with previous workers until it is rotated to be in an equivalent setting. The unit cell used here (i.e. Cmcm transformed

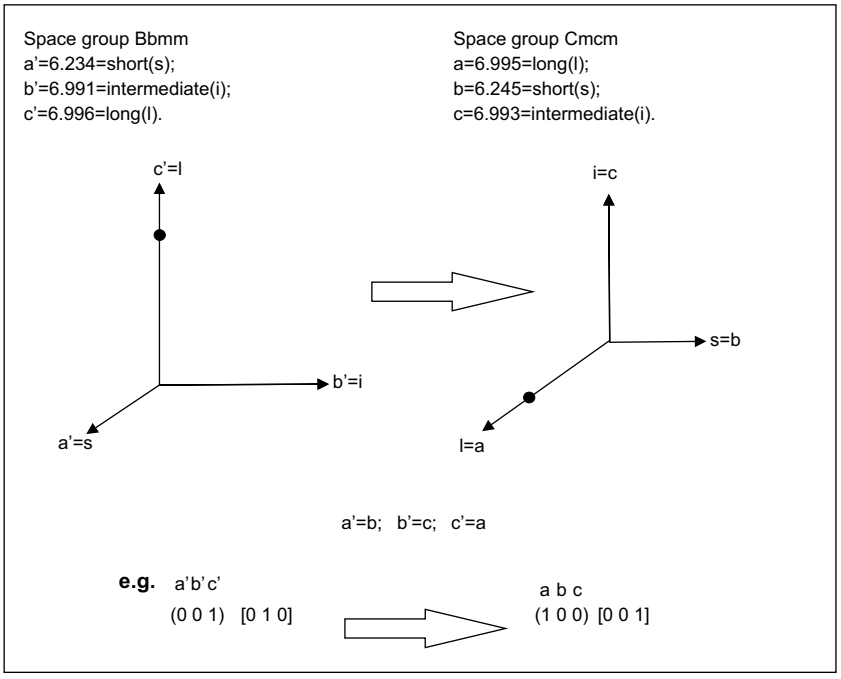

Fig. 3. Diagrammatic representation of the method used to convert previous authors slip systems with a space group setting of Bbmm to the space group setting Cmcm used in this study. The black dot is a reference point to highlight the changes that occur to the position of the axes when the conversion is applied.

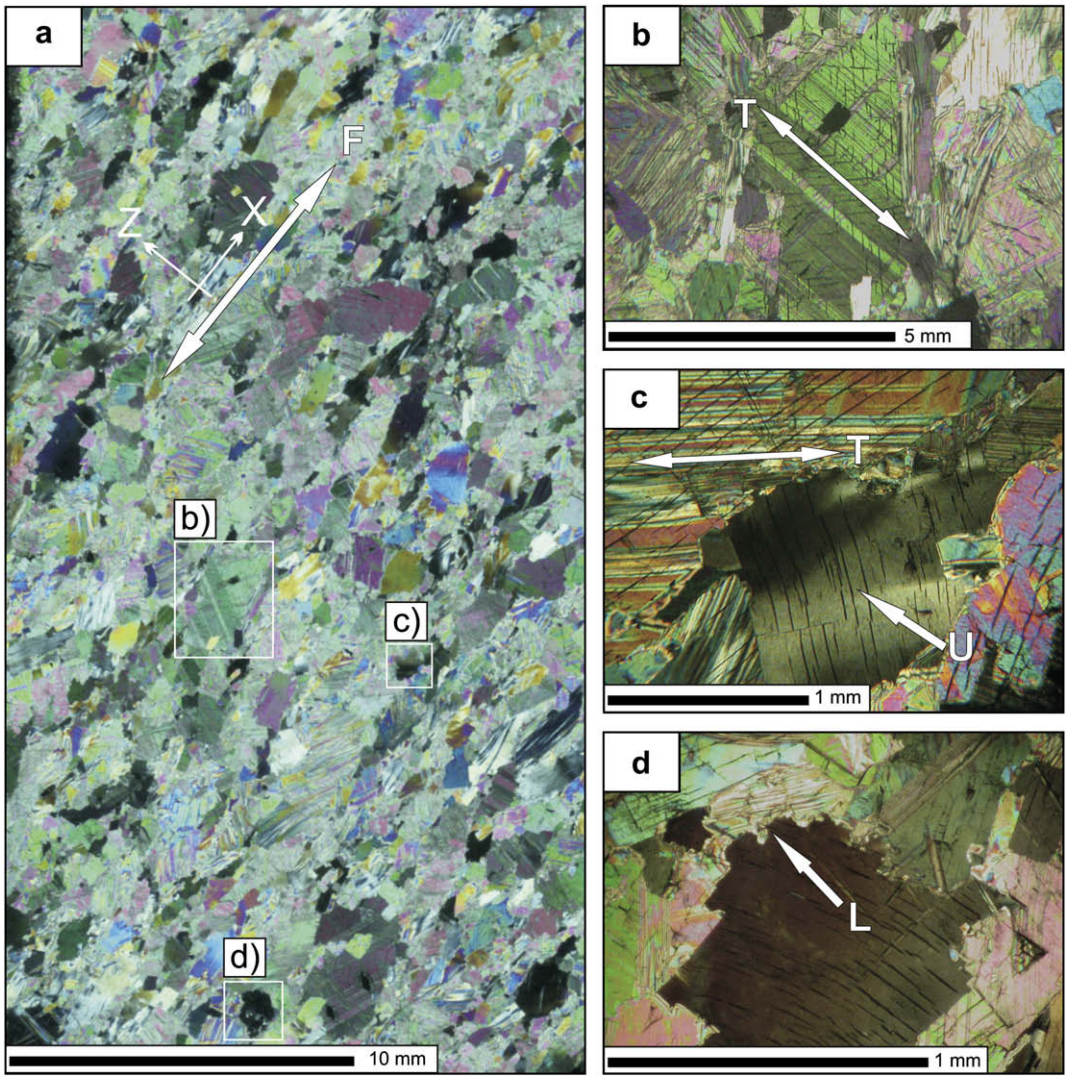

Fig. 4. (a) Crossed polarized light micrograph of the general microstructure within the samples. Arrow labelled F indicates shape preferred orientation of the anhydrite crystals which is taken to be the intersection of the foliation plane with the thin section surface, the *Z–X* indicates the reference frame used for the samples; (b) enlarged micrograph of the boxed area in (a). Arrow labelled T indicates the orientation of the twinning seen; (c) enlarged micrograph of the boxed area in (a). Arrow labelled U points to undulose extinction, arrow labelled T indicates twinning; (d) arrow labelled L points to lobate grain boundaries. NB : Enlarged micrographs (b)–(d) may be rotated with respect to (a).

from Hawthrone and Ferguson's (1975) Amma) is generally considered to be the more accurate setting for anhydrite within the crystallographic literature (i.e. Cheng and Zussman, 1963; Hawthorne and Ferguson, 1975) and as this is the first EBSD analysis of anhydrite it is envisaged that future authors may find it necessary to use the same setting as in this paper (see Appendix A for further details). The rotation used to convert previously recognized slip systems in to the same setting as this work is represented in Fig. 3.

4. Results

4.1. Optical microscopy

The samples are foliated, with an average grain size of 500 μm, and predominately composed of anhydrite (95%) with lesser amounts of fine grained (<50 μm), rounded dolomite. A shape preferred orientation of the anhydrite crystals (Fig. 4a) and a slightly higher concentration of dolomite grains in some planes highlights the foliation (seen in Fig. 1c as slightly darker bands). Between 60 and 85% of the crystals show twinning (Fig. 4b), which is repeated and lamella-like, but which shows no preferential alignment. The twins often have tapering terminations and are sometimes curved. Undulose extinction is also common (Fig. 4c). Grain boundaries are irregular but are often parallel or approximately orthogonal to cleavage planes indicating that there is some crystallographic control to their form. Some grain boundaries exhibit a lobate appearance (Fig. 4d). A summary of the samples used and their properties can be found in Table 1a.

4.2. EBSD analysis

4.2.1. Grain distortions

Texture component maps are used to show the misorientation across individual anhydrite crystals from a reference orientation within each of the four sections studied (Fig. 5). They show significant crystallographic distortions across grains (Fig. 5a). The distortion is gradual and sweeping. Vertical and horizontal misorientation profiles through the distorted grains show a smooth increase in the misorientation angle that ranges between 4° and 18° (Fig. 5b). In some cases a difference is seen between the degree of misorientation in the horizontal and vertical profiles and pole figures, this is a function of sampling through zones of changing

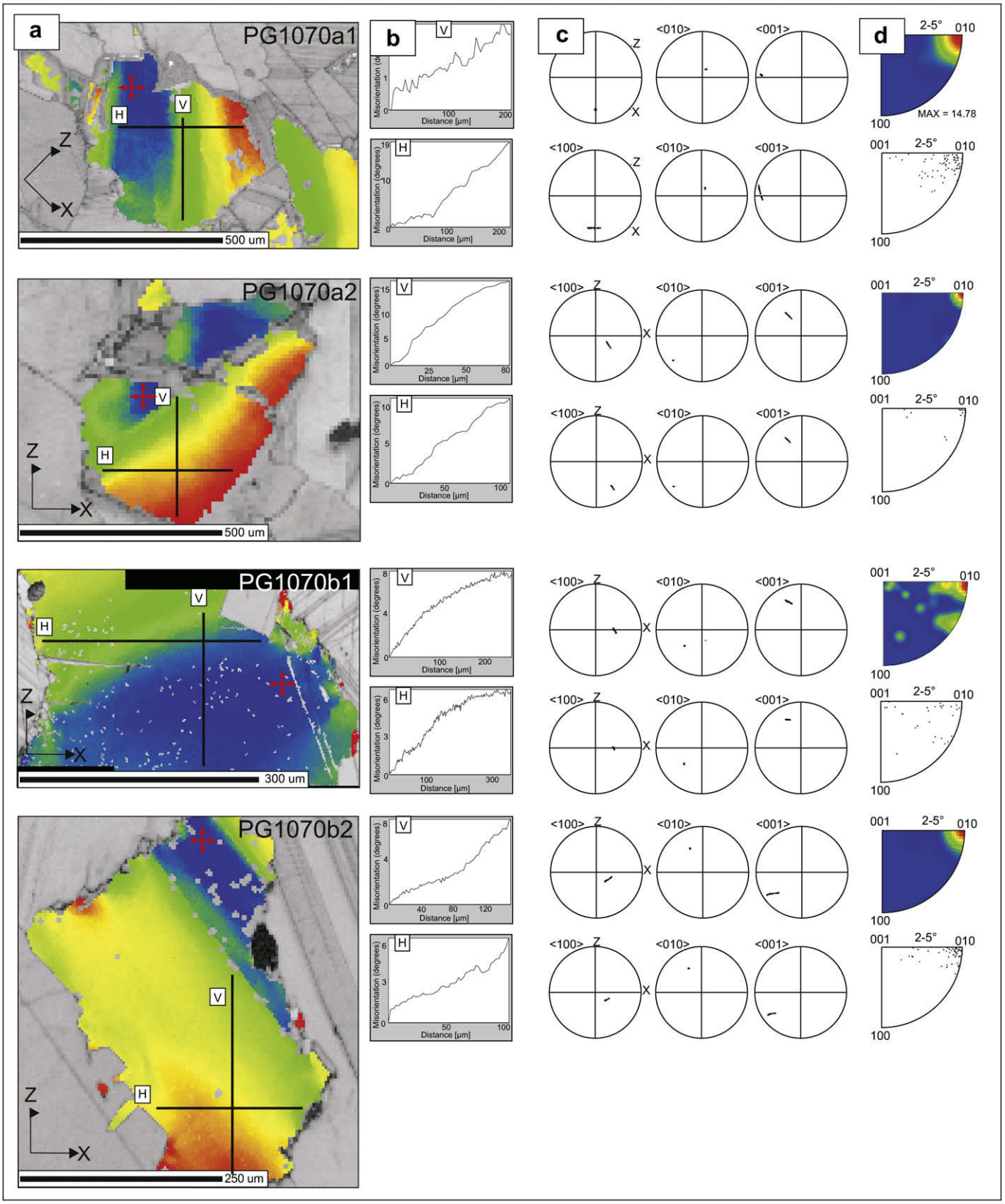

Fig. 5. (a) Band contrast and texture component maps of distorted grains from the four samples analyzed. Note the continuous misorientation across each grain. V and H are the areas where vertical and horizontal data subsets were taken. The red cross in each map indicates the starting reference point to which all other measurements are relative; (b) vertical and horizontal misorientation profiles highlighting the continuous misorientation, profiles taken along the transects indicated in (a); (c) equal angle, upper hemisphere pole figure of the V and H data subsets, ⟨100⟩, ⟨010⟩ and ⟨001⟩ directions are plotted. A clear misorientation axis of ⟨010⟩ and corresponding small circle dispersions in ⟨100⟩ and ⟨001⟩ can be observed; (d) pole figure of rotation axes in crystal co-ordinates displaying the entire data set for each grain for misorientations between 2 and 5°. Contoured and scattered data are shown.

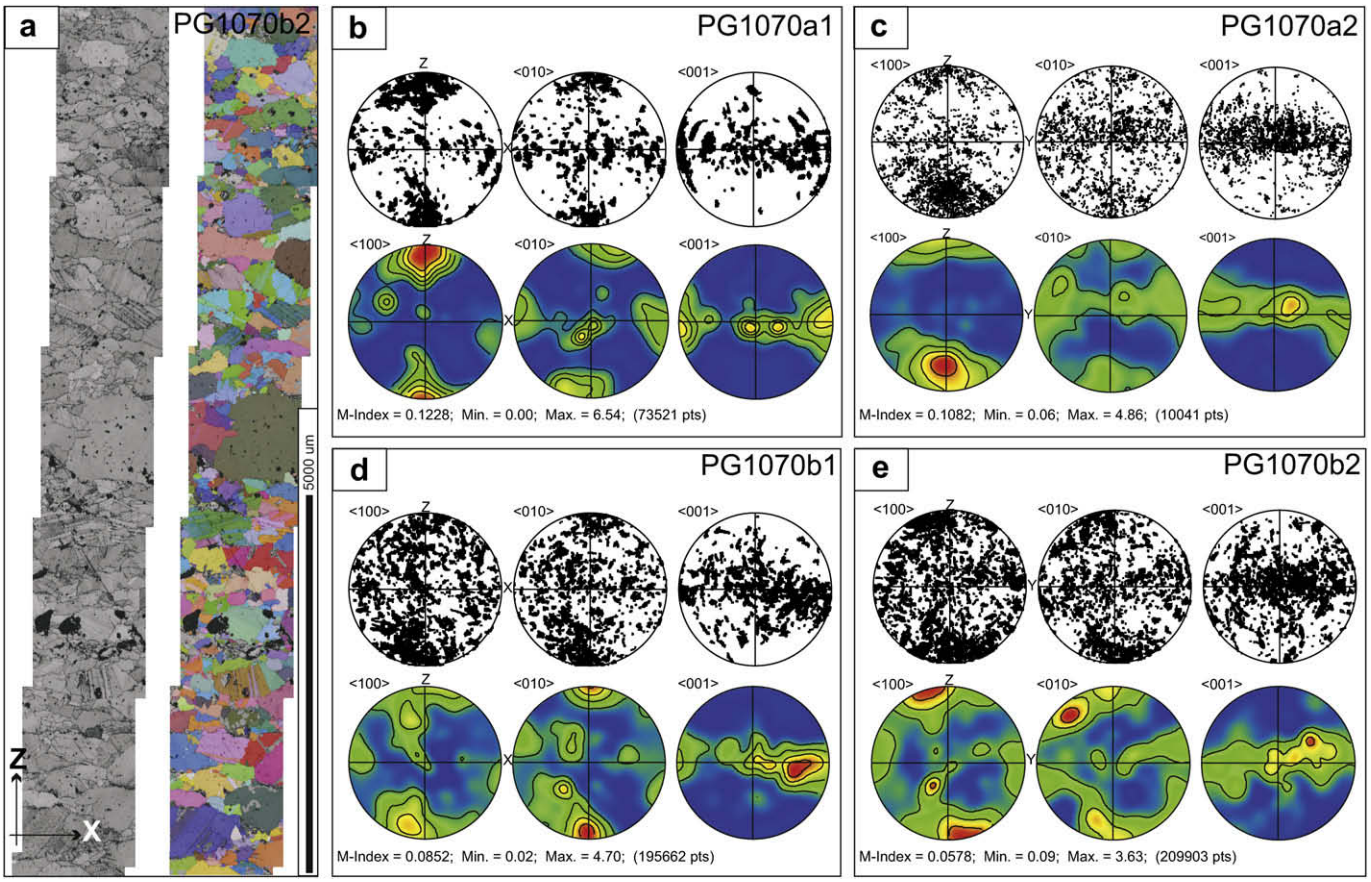

Fig. 6. (a) Example of the area mapped for CPO determination, band contrast and all Euler maps are shown ; foliation is horizontal, parallel to *X*; (b) –(e) each of the four figures displays the CPO for the full data set and are plotted as scattered data and contoured data, on equal area, upper hemisphere, stereographic projections . Density of the contoured pole figures (half width 25°; cluster size 5°) is given as multiples of uniform distribution (MUD) with each contour line representing an increment of 1 up to the stated maximum; (b) and (d) are orientated perpendicular to (c) and (e) and in all cases the foliation is horizontal.

misorientation or through zones with constant misorientation – as is seen in sample PG1070a1 (Fig. 5) where the vertical line is sampling a zone with constant misorientation and the horizontal line is sampling through a continuum of changing misorientation. Stereographic projections of the ⟨100⟩, ⟨010⟩ and ⟨001⟩ directions from a 1 pixel wide horizontal and vertical transect of orientation data (Fig. 5c) show that there is a clear and consistent misorientation around ⟨010⟩, with corresponding dispersions of ⟨100⟩ and ⟨001⟩. Misorientation data for each grain of interest are plotted in a crystal reference frame (Fig. 5d) (i.e. inverse pole figure) and in all cases a clear clustering of points around [010] were observed.

4.2.2. Crystallographic preferred orientation

Low magnification (×50) and large step size (25 μm) maps were acquired perpendicular to the foliation planes (Fig. 6a). Pole figures of the data (full data set) show a clustering of ⟨100⟩ axes perpendicular to the foliation plane. A weak clustering of ⟨010⟩ axes perpendicular to the foliation is also seen in all four data sets. There is also a girdle-like distribution of data in the ⟨001⟩ pole figures parallel to foliation and along this girdle there is a weak point maximum in approximately the same orientation in all four data sets (thin sections a1 and b1 are perpendicular to a2 and b2). No lineation can be defined for these samples, so it is not clear what the relationship of the ⟨100⟩ maximum to lineation is. All samples show a very similar crystallographic preferred orientation.

4.2.3. Twinning

Twinning is observed throughout all the specimens (Fig. 7a). The twins occur as a rotation of the [100] by 83.5° around an axis parallel to [001]. Pole figures of the "host" and "twin" (Fig. 7b) domains in the single grain highlighted in Fig. 7a shows a switch between (100) and (010). The common twin plane within these samples is (110). To try to determine whether twinning is contributing to the bulk CPO observed, pole figures of (110) in twinned grains from data collected for CPO orientation analysis were plotted (Fig. 7c–f). The pole figures show a slight preferred orientation.

5. Discussion

Initial interpretations of the microstructures observed using optical light microscopy suggest that the presence of undulose extinction and grain distortions is indicative of intracrystalline deformation and high dislocation densities. The presence of lobate and irregular high angle grain boundaries could indicate that at least some dynamic recrystallization by grain boundary bulging migration has taken place. Twins with tapered terminations and curved boundaries could be indicative of mechanical twinning. Initial interpretations of the microstructures resolved using EBSD show a continuous misorientation across individual crystals. This may imply that relatively little recovery has happened and that intracrystalline distortion is either due to randomly distributed dislocations (with an excess of one sign) or distributed dislocations walls that cannot be resolved at the scale of the EBSD analyses. The CPO observed in these rocks is evidence that dislocation glide and/or creep are at least contributing deformation mechanisms.

As previous workers based their analyses on a different initial unit cell, to compare directly the results from this study with

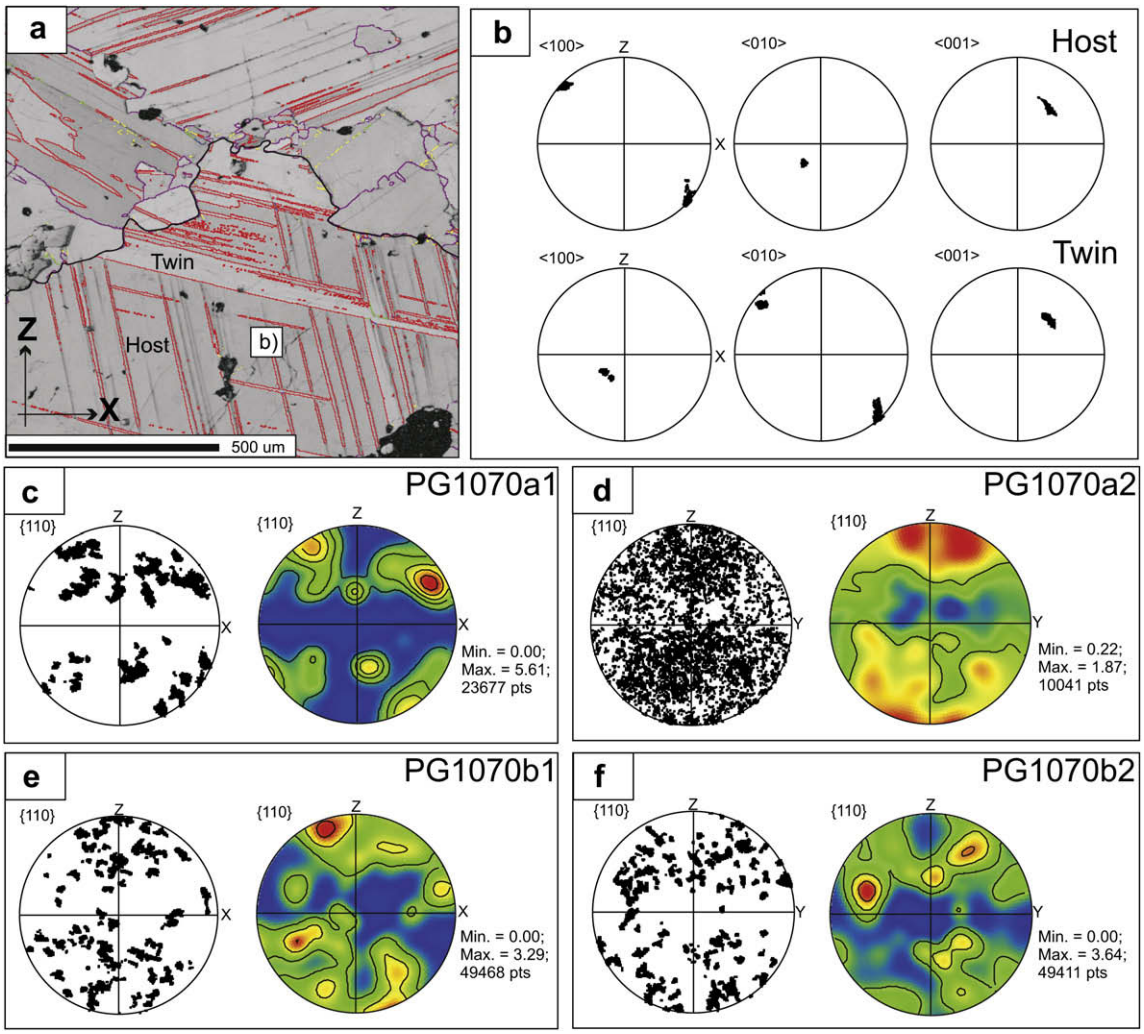

Fig. 7. (a) Band contrast map of an example of the twinning observed, twin boundaries are highlighted in red, >2° grain boundaries are shown in yellow, >5° grain boundaries in green, >20° grain boundaries in purple. The solid black line outlines the grain used for twin and host pole figures in (b). (b) Pole figures showing the reorientation relationship of twinned domains and host domains within a single grain, note the switch between ⟨100⟩ and ⟨010⟩ in the twin and host . (c) -(f) Scattered data and contoured pole figures showing {110} twin plane data from orientation maps previously collected to analyze CPOs. Only data points from twinned grains are included in pole figures, expect for (d) where the full CPO data set is plotted. Density of the contoured pole figures (half width 25°; cluster size 5°) is given as multiples of uniform distribution (MUD) with each contour line representing an increment of 1 up to the stated maximum. Data appears to be randomly distributed, indicating that twinning is showing no systematic alignment. (c) and (e) are orientated perpendicular to (d) and (f) and in all cases the foliation is horizontal.

previous studies a rotation of their data into the same orientation as our data is needed. Once this rotation is carried out it can be seen that one of the previously reported slip systems (Fig. 2 and Table 2) can be reconciled with the anhydrite CPOs observed in this study but it can also simply explain the distortions observed within grains.

Misorientation axes may be used to constrain important slip systems (Lloyd and Freeman, 1991; Lloyd and Freeman, 1994; Leiss and Barber, 1999; Prior et al., 2002). The previously reported slip systems were inferred using misorientation axes derived from CPO measurements. Using EBSD, the orientation maps collected not only measure the full crystallographic orientation of each point, but also constrain the orientation of low angle boundaries, an alternative analysis of slip systems can be made (Prior et al., 2002).

The 2D orientation of the trends of misorientation in the texture component maps are taken to be the orientation of the boundary trace which would be produced if the distortions were a low angle boundary within the grain. The insets in Fig. 8d–g show the trace of the trends of misorientations seen within the grains studied that give clear distortions around [010] (Fig. 5c). To make further interpretations, an assumption is needed as to whether the data best fits with a tilt boundary model or a twist boundary model (Lloyd et al., 1997; Prior et al., 2002). If the boundaries are assumed to be tilt walls then the boundary plane must contain the mapped boundary trace and the misorientation axis (Fig. 8a), whereas if boundaries are twist walls then the misorientation axis must be perpendicular to the boundary (Fig. 8b) (Lloyd et al., 1997; Prior et al., 2002). As Fig. 8c illustrates, in a tilt boundary the misorientation axis must be contained within the slip plane and at 90° to the slip vector, both of which are at a high angle to the boundary plane. In all of the grains analyzed a tilt boundary model best fits the data (Fig. 8d–g) and a twist boundary model can be excluded. Fig. 8d–g shows the solutions that best describe the results. Adhering to the geometrical constraints of the tilt boundary model, the simplest solution to the misorientation data seen in distorted grains is activity on the known slip system of (100)[001] (e.g. Muller et al., 1981; Mainprice et al., 1993) with a consistent rotation axis of [010]. The (100) slip plane is orientated at a high (~90°) to intermediate (~65°) angle to the boundary plane which is a requirement for the tilt boundary model. To constrain further this slip system a physical

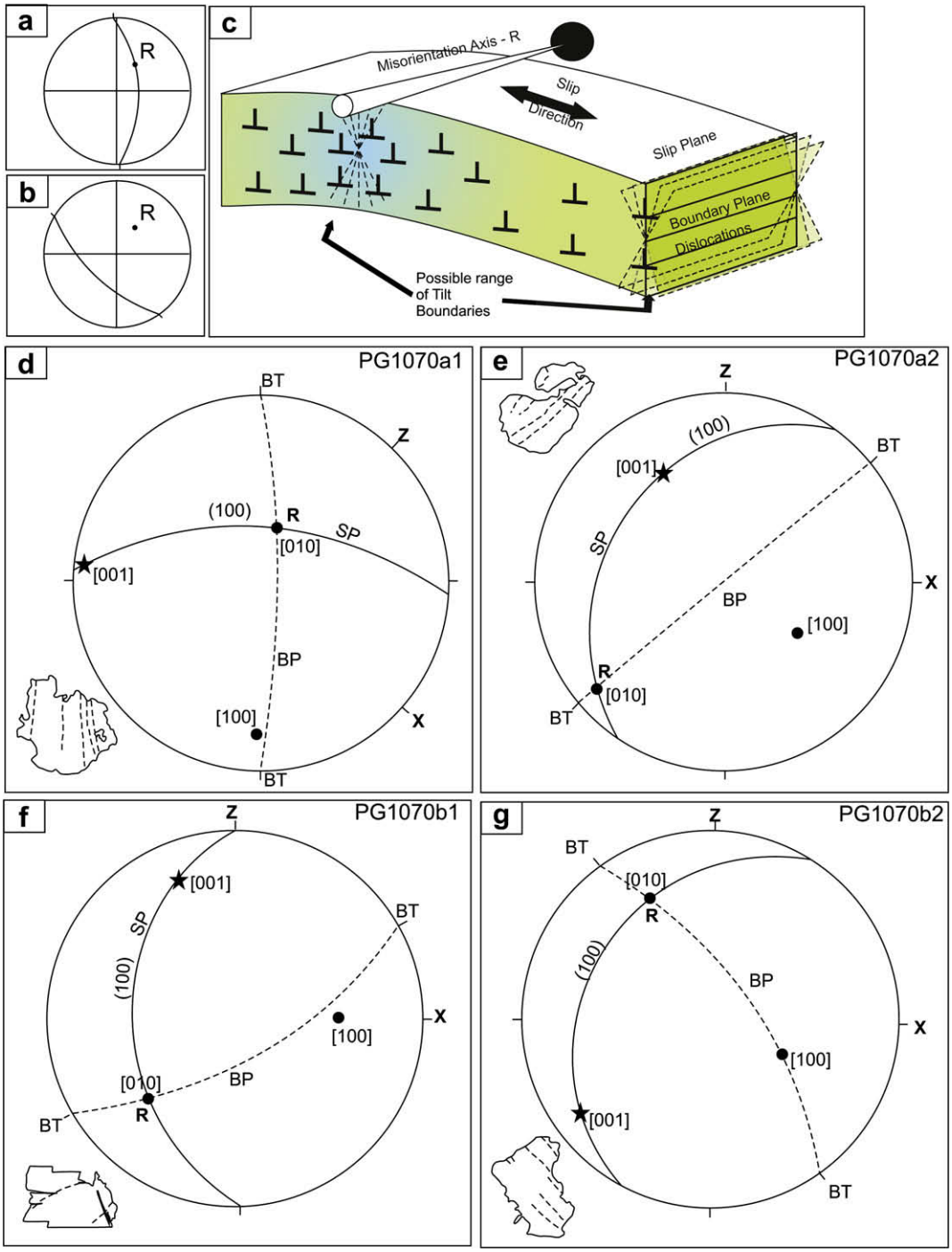

Fig. 8. Dislocation models and interpretative pole figures of the grain distortion data. (a) The great circle shows the approximate boundary plane if the boundaries in (d) are tilt walls, lines extending outside the primitive are the expected boundary trace . (b) The great circle shows the approximate boundary plane (orthogonal to the misorientation axis) predicted if the boundaries in (d) are twist walls, lines extending outside the primitive are the expected boundary trace . (c) Modified after Prior et al. (2002), a 3D cartoon representation of a tilt boundary model showing the relative orientations of the slip plane, slip direction, boundary plane and misorientation axis . (d) –(g) Equal angle, stereographic projections of the slip systems that can fit the data. Insets are a schematic of the distorted grain to show the orientation of the boundary trace. Solid black circles represent the data from the misorientation analysis pole figures, R is the rotation/misorientation axis, solid black stars are the interpreted slip vectors, BT is the boundary trace, BP is the boundary plane, [ ] represent directions and ( ) represent planes.

measure of the orientation of the boundary plane would be needed (using an optical microscope fitted with a universal stage), however this is not possible in this case as the distortions are too diffuse to be resolved into planes. It has been considered that complex, coupled activity on the (201)[1-1-2] and (201)[11-2] slip systems could be used to explain some of the dispersions seen, although when each of these slip systems is used in isolation they are not consistent with the data.

CPO data show a concentration in the ⟨100⟩ pole figure indicating a preferential alignment of *a*-axes perpendicular to the foliation. This is interpreted to be indicative of slip on (100). The weak maximum in the ⟨010⟩ pole figures is suggestive that twinning is contributing slightly to the CPO (see discussion below), resulting from the switch between ⟨100⟩ and ⟨010⟩. This would be consistent with the observation made by Mainprice et al. (1993) who noted that if twinning was a dominant process for fabric

Table 3
Complete crystallographic data for anhydrite, gypsum and bassanite.

Anhydrite original				Anhydrite transformed			
Reference	Hawthorne and Ferguson, 1975			Reference	Hawthorne and Ferguson, 1975		
Space group no.	*a*	*b*	*c*	**Space group no.**	*a*	*b*	*C*
63	6.993	6.995	6.245	63	6.995	6.245	6.993
Space group	*α*	*β*	*γ*	**Space group**	*α*	*β*	*Γ*
amma	90	90	90	Cmcm	90	90	90
Point group	Schoenflies			**Point group**	Schoenflies		
mmm	D2h^17			mmm	D2h^17		
Atoms	*x*	*y*	*z*	**Atoms**	*x*	*y*	*Z*
Ca	0.75	0	0.3476	Ca	0	0.3476	0.75
S	0.25	0	0.1556	S	0	0.1556	0.25
O	0.25	0.1699	0.0162	O	0.1699	0.0162	0.25
O	0.0819	0	0.02975	O	0	0.02975	0.0819
Gypsum original				Gypsum transformed			
Reference	Boeyens and Ichhram, 2002			Reference	Boeyens and Ichhram, 2002		
Space group no.	*a*	*b*	*c*	**Space group no.**	*a*	*b*	*C*
15	6.284	15.2	6.523	15	6.284	15.2	6.523
Space group	*α*	*β*	*γ*	**Space group**	*α*	*β*	*Γ*
C2/c	90	127.41	90	C2/c	90	127.41	90
Point group	Schoenflies			**Point group**	Schoenflies		
2/m	C2h^6			2/m	C2h^6		
Atoms	*x*	*y*	*z*	**Atoms**	*x*	*y*	*Z*
Ca	0.5	0.07956	0.75	Ca	0.5	0.07956	0.75
S	0	0.07724	0.75	S	0	0.07724	0.75
O	0.0372	0.13198	0.5872	O	0.0372	0.13198	0.5872
O	0.2424	0.02211	0.9092	O	0.2424	0.02211	0.9092
O	0.6202	0.18197	0.0784	O	0.6202	0.18197	0.0784
H	0.749	0.162	0.251	H	0.749	0.162	0.251
H	0.584	0.235	0.073	H	0.584	0.235	0.073
Bassanite original				Bassanite transformed			
Reference	Bezou et al., 1995			Reference	Bezou et al., 1995		
Space group no.	*a*	*b*	*c*	**Space group no.**	*a*	*b*	*C*
5	12.0317	6.9269	12.6712	5	17.4323	6.9269	12.0317
Space group	*α*	*β*	*γ*	**Space group**	*α*	*β*	*Γ*
I 121	90	90.27	90	C2	90	133.38	90
Point group	Schoenflies			**Point group**	Schoenflies		
2	C3^2			2	C3^2		
Atoms	*x*	*y*	*z*	**Atoms**	*x*	*y*	*Z*
Ca	0	0.015	0.5	Ca	−0.5	0.015	−0.5
Ca	0.718	0.177	0.157	Ca	−0.157	0.177	0.561
Ca	0.263	0.218	0.337	Ca	0.337	0.218	−0.074
Ca	0	0	0	Ca	0	0	0
S	−0.002	0.024	0.253	S	−0.253	0.024	−0.255
S	0.723	0.191	0.417	S	−0.417	0.191	0.306
S	0.276	0.204	0.087	S	−0.087	0.204	0.189
O	0.072	0.156	0.315	O	−0.315	0.156	−0.243
O	0.063	−0.102	0.181	O	−0.181	−0.102	−0.118
O	−0.079	0.13	0.18	O	−0.18	0.13	−0.259
O	−0.065	−0.105	0.325	O	−0.325	−0.105	−0.39
O	0.738	0.338	0.333	O	−0.333	0.338	0.405
O	0.629	0.232	0.489	O	−0.489	0.232	0.14
O	0.825	0.18	0.486	O	−0.486	0.18	0.339
O	0.706	−0.003	0.01646	O	−0.365	−0.003	0.341
O	0.226	0.364	0.148	O	−0.148	0.364	0.078
O	0.376	0.244	0.022	O	−0.022	0.244	0.354
O	0.194	0.131	0.007	O	−0.007	0.131	0.187
O	0.299	0.042	0.161	O	−0.161	0.042	0.138
O	0.049	0.503	0.65	O	−0.65	0.503	−0.601
O	0	0.349	0	O	0	0.349	0
H	−0.049	0.436	0.039	H	−0.039	0.436	−0.088
H	−0.021	0.567	0.659	H	−0.659	0.567	−0.68
H	0.049	0.4	0.703	H	−0.703	0.4	−0.654

Original data sourced from Hawthorne and Ferguson (1975), Boeyens and Ichhram (2002) and Bezou et al. (1995).

development a concentration of ⟨010⟩ axes normal to foliation (i.e. a clustering around *Z* in this study) would be seen. The girdle-like spread of data seen in the ⟨001⟩ pole figures is consistent with the observation of oblate shaped grains resulting from a flattening strain. The weak point maximum seen along this girdle could be interpreted as being the slip vector for grains which are favourably orientated within the plane of flattening, this would result in a slip system of (100)[001]. This would support, and be consistent with, one of the slip systems interpreted from the grain distortion data and also be equivalent to the (100)[001] slip system determined by previous authors (i.e. Mainprice et al., 1993; Heidelbach et al., 2001).

Twinning within these samples is predominantly on (110) (which is equivalent to the (101) twins from the Bbmm space group setting of previous studies and is also equivalent to the (011) twins in the space group Amma published by Hawthorne and Ferguson

(1975)) It can be illustrated from the "host" domain and "twin" domain pole figures that twinning essentially flips (100) and (010) suggesting that if twinning was the dominant deformation mechanism a strong CPO signal would be observed in ⟨010⟩ pole figures. If the pole figures of the twin planes of twinned crystals within these samples are considered (Fig. 7c–f), the spread of data shows slight clustering near *Z* similar to the concentration of data points in the ⟨100⟩ and ⟨010⟩ pole figures in Fig. 6. NB: Fig. 7d is a plot of all grains and not just twinned grains as the data was collected at a coarse level (for bulk CPO analysis) and therefore twinned grains could not be distinguished from untwinned grains, but it is included for comparison. A significantly strong preferred orientation of twin planes in all samples is not seen, and therefore is in contrast to previous studies (Ramez, 1976b; Muller et al., 1981; Mainprice et al., 1993). However, as a weak signal of twinning does appear in the CPO data (Fig. 6b–e), it can be determined that twinning in these samples is not only an important deformation mechanism for accommodating some of the deformation but it contributed slightly to the overall CPO development.

6. Conclusions

Interpretation of orientation and misorientation data from the microstructural analysis of coarse grained anhydrite rocks from the Triassic Evaporites of the central Italian Apennines using EBSD analysis allows the following conclusions to be drawn:

1. There is a marked crystallographic preferred orientation that is consistent with the activity of the (100)[001] slip system dominating grain rotations during deformation. This confirms the recognized easy slip system for anhydrite;
2. Misorientation analysis has identified the (100)[001] slip system as the dominant slip system controlling the internal distortions within anhydrite;
3. Twinning is likely to have accommodated some of the deformation and may have a limited effect on the texture measured;
4. Intracrystalline deformation evidenced by grain distortions and undulose extinction are best explained by the presence of dislocations. Because distortions are gradual it is likely that little recovery has happened in these grains;
5. Lobate and irregular boundaries suggest that a degree of dynamic recrystallization by grain boundary bulging may have taken place.

Acknowledgements

We thank Nicola de Paola and Cristiano Collettini for providing the samples and background for this study. A NERC studentship, research grant number NER/S/A/2005/13332 and two NERC grants NER/A/S/2001/01181 and NE/C002938/1, funded this work. Mark Pearce is thanked for his help with and numerous discussions on plotting anhydrite crystal structure on to stereographic projections. We are grateful for the detailed and helpful reviews from Florian Heidelbach and Luigi Burlini which improved the original manuscript.

Appendix A. Ca-sulphate crystallography

In order to perform EBSD analysis it is essential to know the crystallography of the minerals of interest so that the software used (in this case Channel 5) can relate the diffraction pattern produced on the phosphor screen with solutions related to different crystallographic orientations. Crystallographic reference files for most rock forming minerals have been organized on to databases, e.g. American Mineralogist, however the relevant Ca-sulphate (anhydrite, bassanite, gypsum) files are not.

Anhydrite is orthorhombic and its structure is best represented by the space group Amma (Hawthorne and Ferguson, 1975) and point group 2/m 2/m 2/m. However, this space group is not stored in the Channel5 crystal file creator utility Twist. The space group Amma is an extended Hermann–Mauguin symbol representing one of six possible settings for the same unit cell (International Table of Crystallography; Hahn, 2005). The standard Hermann–Mauguin notation (used in Twist) uses the setting *a b c* (basis vectors) and the space group Cmcm. Whereas the space group Amma has a setting of *c a b*. Therefore, transformation of the coordinate system and the unit cell relative to the crystal structure is needed. To achieve this, a transformation matrix routine made available by the Bilbao Crystallographic Server (Aroyo et al., 2006a,b) was used. Crystal files were created for anhydrite with both original data and then transformed data so that their accuracy could be tested against real EBSD patterns collected from the samples (see Table 3).

References

Aroyo, M.I., Kirov, A., Capillas, C., Perez-Mato, J.M., Wondratschek, H., 2006a. Bilbao Crystallographic Server ii: Representations of crystallographic point groups and space groups. Acta Crystallography A62, 115–128.

Aroyo, M.I., Perez-Mato, J.M., Capillas, C., Kroumova, E., Ivantchev, S., Madariaga, G., Kirov, A., Wondratschek, H., 2006b. Bilbao crystallographic server i: Databases and crystallographic computing programs. Zeitschrift fuer Kristallographie 221 (1), 15–27.

Bally, A., Burbi, L., Cooper, C., Ghelardoni, R., 1986. Balanced sections and seismic reflection profiles across the Central Apennines. Memorie della Societa Geologica Italiana 35, 257–310.

Barchi, M.R., De Feyter, A., Magnani, M., Minelli, G., Pialli, G., Sotera, B., 1998a. The structural cycle of the Umbria-Marche fold and thrust belt. Memorie della Societa Geologica Italiana 52, 557–578.

Bezou, C., Nonat, A., Mutin, J.C., Norlund Christensen, A., Lehmann, M., 1995. Investigation of the crystal structure of [gamma]-CaSO4, CaSO4.0.5 H2O, and CaSO4.0.6 H2O by powder diffraction methods. Journal of Solid State Chemistry 117 (1), 165–176.

Boeyens, J.C.A., Ichhram, V.V.H., 2002. Redetermination of the crystal structure of calcium sulphate dihydrate, CaSO4–2H2O. Zeitschrift fuer Kristallographie 27, 9–10.

Cheng, G.C.H., Zussman, J., 1963. The crystal structure of anhydrite (CaSO4). Acta Crystallographica 16, 767–769.

De Paola, N., Collettini, C., Faulkner, D.R., Trippetta, F., 2008. Fault zone architecture and deformation processes within evaporitic rocks in the upper crust. Tectonics 27, TC4017.

Dell'Angelo, L.N., Olgaard, D.L., 1995. Experimental deformation of fine-grained anhydrite: evidence for dislocation and diffusion creep. Journal of Geophysical Research 100, 15425–15440.

Elter, P., Giglia, G., Tongiorgi, M., Trevisan, L., 1975. Tensional and compressional areas in the recent (Tortian to Present) evolution of the Northan Apennines. Bollettino di Geofisica Teorica ed Applicata 17, 3–18.

Hahn, T. (Ed.), 2005. International Tables for Crystallography, vol. A: Space Group Symmetry. International Tables for Crystallography, Springer.

Hartman, P., 1989. On the unit cell dimensions and bond lengths of anhydrite. European Journal of Mineralogy 1, 721–722.

Hawthorne, F.C., Ferguson, R.B., 1975. Anhydrous sulphates. II. Refinement of the crystal structure of anhydrite. Canadian Mineralogist 13, 289–292.

Heidelbach, F., Stretton, I.C., Kunze, K., 2001. Texture development of polycrystalline anhydrite experimentally deformed in torsion. International Journal of Earth Sciences 90, 118–126.

Hohne, E., 1963. A more accurate determination of the crystal structure of anhydrite. Soviet Physics – Crystallography 7, 599–569.

Jolivet, L., Faccenna, C., Goffe, B., Mattei, M., Rossetti, M., Brunet, F., Storti, F., Funiciello, R., Cadel, J.P., D'Agostino, N., Parra, T., 1998. Midcrustal shear zones in postorogenic extension: example from the northern Tyrrhenian Sea. Journal of Geophysical Research 103 (B6), 12123–12160.

Jordan, P., Nuesch, R., 1989. Deformation structures in the Muschelkalk anhydrites of the Schafisheim Well (Jura Overthrust, northern Switzerland). Eclogae Geologicae Helvetiae 82 (2), 429–454.

Klassen-Neklyudova, M.V., 1964. Mechanical Twinning of Crystals. Consultants Bureau, New York, pp. 1-87.

Laubscher, H.P., 1975. Viscous components in Jura folding. Tectonophysics 27 (3), 239–254.

Leiss, B., Barber, D.J., 1999. Mechanisms of dynamic recrystallization in naturally deformed dolomite inferred from EBSP analyses. Tectonophysics 303 (1-4), 51–69.

Lloyd, G.E., Farmer, A.B., Mainprice, D., 1997. Misorientation analysis and the formation and orientation of subgrain and grain boundaries. Tectonophysics 279 (1-4), 55–78.

Lloyd, G.E., Freeman, B., 1991. SEM electron channelling analysis of dynamic recrystallization in a quartz grain. Journal of Structural Geology 13 (8), 945–953.
Lloyd, G.E., Freeman, B., 1994. Dynamic recrystallization of quartz under greenschist conditions. Journal of Structural Geology 16 (6), 867–881.
Mainprice, D., Bouchez, J.-L., Casey, M., Dervi, P., 1993. Quantitative texture analysis of naturally deformed anhydrite by neutron diffraction texture goniometry. Journal of Structural Geology 15 (6), 793–804.
Marcoux, J., Brun, J.P., Burg, J.P., Ricou, L.E., 1987. Shear structures in anhydrite at the base of thrust sheets (Antalya, Southern Turkey). Journal of Structural Geology 9 (5-6), 555–561.
Miller, S.A., Collettini, C., Chiaraluce, L., Cocco, M., Barchi, M., Kaus, B.J.P., 2004. Aftershocks driven by a high-pressure CO_2 source at depth. Nature 427 (6976), 724–727.
Mugge, O., 1883. Uber translatioen und verwandte erscheinungen in kristallen. Neues Jahrb. Mineral 1, 71–162.
Muller, W.H., Schmid, S.M., Briegel, U., 1981. Deformation experiments on anhydrite rocks of different grain sizes: rheology and microfabric. Tectonophysics 78 (1-4), 527–543.
Pauselli, C., Barchi, M.R., Federico, C., Magnani, B.M., Minelli, G., 2006. The crustal structure of the Northern Apennines (Central Italy): an insight by the CROP3 seismic line. American Journal of Science 306, 428–450.
Prior, D.J., 1999. Problems in determining the misorientation axes, for small angular misorientations, using electron backscatter diffraction in the SEM. Journal of Microscopy 195 (3), 217–225.
Prior, D.J., Wheeler, J., Peruzzo, L., Spiess, R., Storey, C., 2002. Some garnet microstructures: an illustration of the potential of orientation maps and misorientation analysis in microstructural studies. Journal of Structural Geology 24 (6-7), 999–1011.
Ramez, M.R.H., 1976b. Fabric changes in experimentally deformed anhydrite rocks. Neues Jahrb. Mineral 128, 89–113.
Schmidt, N.H., Olesen, N.O., 1989. Computer-aided determination of crystal-lattice orientation from electon-channeling patterns in the SEM. Canadian Mineralogist 27, 15–22.
Wenk, H.-R., Bulakh, A. (2004). Minerals – Their Constitution and Origin, Cambridge.